Watershed and multimodal data for brain vessel segmentation: Application to the superior sagittal sinus

Nicolas Passat, Christian Ronse, Joseph Baruthio, Jean-Paul Armspach, Jack Foucher

Watershed and Multimodal Data for Brain Vessel Segmentation: Application to the Superior Sagittal Sinus

N. Passat [a,b,*], C. Ronse [a], J. Baruthio [b], J.-P. Armspach [b],
J. Foucher [c]

[a]*LSIIT, Laboratoire des Sciences de l'Image, de l'Informatique et de la Télédétection,
UMR 7005 CNRS/ULP, Strasbourg 1 University,
Parc d'Innovation, Bd Sébastien Brant BP 10413, F-67412 Illkirch Cedex, France*

[b]*IPB-LNV, Institut de Physique Biologique - Laboratoire de Neuroimagerie in Vivo,
UMR 7004 CNRS/ULP, Strasbourg 1 University,
Hôpital Civil, 4 rue Kirschleger, F-67085 Strasbourg Cedex, France*

[c]*Unité de Recherche en Psychopathologie et Pharmacologie de la Cognition,
U405 INSERM,
Hôpital Civil, 1 place de l'Hôpital, BP 426, F-67091 Strasbourg Cedex, France*

Abstract

Magnetic resonance angiography (MRA) provides 3-dimensional data of vascular structures by visualising the flowing blood signal. Algorithms dedicated to vessel segmentation generally detect the cerebral vascular tree by only seeking this high intensity blood signal in MRA data. The method presented in this paper proposes a different strategy which consists in using both MRA and classical MRI in order to integrate *a-priori* anatomical knowledge for guidance of the vessel segmentation process. It then uses mathematical morphology tools to carry out a simultaneous segmentation of both blood signal in MRA and blood and wall signal in MRI, enabling to take advantage of a larger amount of information than previously proposed methods. This method is dedicated to the superior sagittal sinus segmentation; however similar strategies could be considered for segmentation of other vascular structures. It has been performed on a database composed of 9 couples of MRA and MRI, providing results which have been validated and compared to other ones obtained with a region-growing algorithm. Their validation tends to prove that the proposed method is reliable even when the vascular signal is inhomogeneous or contains artifacts.

Key words: vessel segmentation, watershed segmentation, *a-priori* knowledge integration, magnetic resonance imaging.

---

* Corresponding author: `passat@dpt-info.u-strasbg.fr`.

1   Introduction

Magnetic resonance angiography (MRA) is a family of image acquisition processes [1] frequently used to provide 3D data of cerebral vascular structures. These techniques, including time-of-flight (TOF) [2] and phase-contrast (PC) MRA [3], which are non-irradiant and non-invasive, are then generally used for studying cerebral vascular structures, in order to detect vascular pathologies (stenoses, aneurysms) but also to plan and perform neurosurgical procedures or to detect vessels which can be used as landmarks for functional analysis or magnetic transcranial stimulation procedures.

Many classical image processing tools have been applied to the segmentation of vessels, but very few effort has been spent to the integration of information to for guidance of the proposed methods. Then it might be interesting to explore new kinds of algorithms involving *a-priori* anatomical knowledge. The use of such knowledge, which is a strategy generally proposed by radiologists to guide their own analysis, could then enable to guide automatic vessel segmentation and then to improve their ability to correctly detect vessels. In a previous work [4] a first attempt to use anatomical knowledge as a way to guide a segmentation algorithm has been described. A major breakthrough of this work was the creation of an atlas dividing the human head into different areas presenting homogeneous vessel properties. The use of this atlas enables to store *a-priori* knowledge concerning the vessels located in each area and then to propose *ad hoc* segmentation algorithms guided by this knowledge. This paper describes an algorithm dedicated to one of these areas containing a main vessel of the venous tree: the superior sagittal sinus, a reliable detection of which is of high interest to correctly initialise segmentation of larger brain vascular networks. The research work proposed in the following is an extended and optimised version of the one detailed in [5]. This optimised algorithm is still essentially based on mathematical morphology tools and more especially on watershed segmentation. Moreover it now also uses homotopic reduction which enables to add continuity and regularity constraints during the segmentation process. It is based on *a-priori* anatomical knowledge concerning the relations between the superior sagittal sinus and the neighbouring tissues, and uses both MRA and MRI data in order to take advantage of both acquisition techniques. It uses a slice by slice process, simultaneously segmenting the flowing blood signal in MRA and the blood and vessel wall in MRI.

This paper is organised as follows. In Section 2, previous approaches concerning vessel segmentation and based on mathematical morphology are described. The general methodology of vessel segmentation is also analysed to justify the proposed approach. In Section 3, the different pieces of anatomical knowledge about the superior sagittal sinus and the way to use them in a segmentation process are described. Section 4 provides a detailed presentation of the algorithm. In Section 5, technical details concerning the method and the database used for validation are

given. Section 6 proposes a validation of the method which is tested and compared to a region-growing algorithm. Conclusion and projects are presented in Section 7.

2   Related work

Many vessel segmentation methods devoted to 3D angiographic data have been proposed during the last fifteen years. These methods can be divided into different categories corresponding to the main strategies used to carry out the segmentation (including - but not restricted to - filtering, mathematical morphology, vessel tracking and deformable models). Recent overviews of such segmentation methods are provided in [6,7].

Mathematical morphology has been one of the first kinds of techniques involved in the segmentation of vessels from 3D angiographic data. Indeed, it provides a very complete framework enabling to detect vessels by considering properties related not only to their intensity but also to their shape. The first developed methods based on mathematical morphology were essentially using thresholding. In [8], hysteresis thresholding has then been used prior to description of brain vessels from MRA data. More recently, an adaptive thresholding technique has been proposed in [9] for the same kind of data. Other techniques are based on erosion and dilation. In [10], the binary image of the whole blood pool initially obtained by manual thresholding from an MRA data is processed by a binary opening (erosion followed by a dilation) involving a spherical structuring element, thus providing the small coronary arteries by subtraction. A grey-level version of this method has also been proposed in [11]. Grey-scale skeletonization strategies have also been developed, as the one described in [12], where an acyclic graph is generated from MRA data by using ordered region-growing. More generally, region-growing methods constitute a large part of the proposed segmentation strategies [4,13,14]. More sophisticated
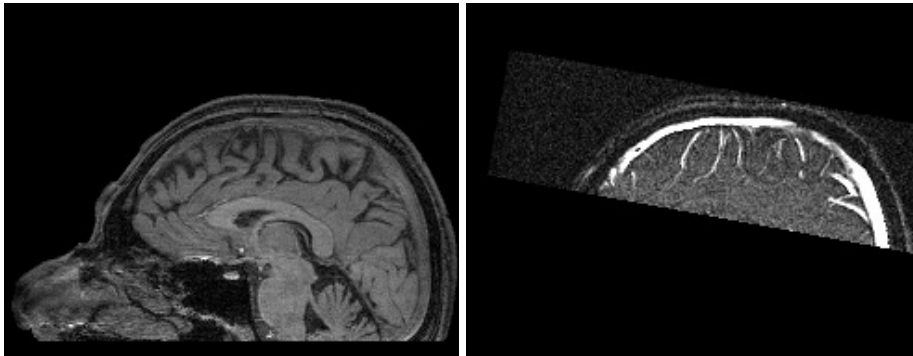

Fig. 1. Left: T_1 MRI sagittal slice of the whole head. Right: MRA sagittal slice of the top of the head. The superior sagittal sinus corresponds to the largest high intensity curve, parallel to the surface of the head. It is also visible in the MRI image, where it corresponds to the homogeneous intensity area between the brain and the skull.

mathematical morphology operators have recently been proposed, as in [15,16], where watershed segmentation is performed on cerebral MRA before classifying the obtained primitives by using fuzzy logic techniques or neural networks. Finally, grey-level hit-or-miss operators have been considered too for vessel segmentation applications, in [17,18] for cerebral MRA analysis and in [19] for liver vasculature detection from CT-scans.

Generally, one can observe that multimodal data are not involved in vessel segmentation processes (based on mathematical morphology or any other kinds of image processing concepts). In [20], a method using both 3D MRA and 2D X-ray images, has been proposed for brain vessel visualisation, taking advantage of the accuracy of X-ray data and of the 3D information provided by MRA data. In [21], another multimodal approach has been developed for reconstruction of 3D vascular data from 2D X-ray images and ultrasound data. Except from these examples, these kinds of methods remain quite unusual. Moreover, the few methods using multimodal data only consider angiographic images, while integration of non-angiographic ones could provide useful information, as shown in [4].

The use of high level *a-priori* knowledge related to the content of the images, is also completely underused. Except in very few examples such as [14] and [17,18] where knowledge about vascular structure topology and about size and orientation of the searched vessels are used to guide the segmentation processes, nearly all the described methods are based on quite simple hypotheses generally linked to the blood signal intensity and the cylindrical shape of the vessels.

Although the use of high level *a-priori* knowledge and multimodal data remain infrequent, it can probably enable to propose efficient segmentation methods, taking advantage of the supplementary information provided by the use of several images visualising different anatomical structures, and of the relations existing between the vascular and non-vascular ones. The algorithm presented hereafter is an example of such a strategy, devoted to the superior sagittal sinus segmentation. It is mainly based on watershed [22] segmentation, and proposes to uses both MRA and MRI to take advantage of anatomical knowledge concerning this part of the cerebral venous tree and its neighbouring cerebral structures.

3 *A-priori* knowledge integration

The superior sagittal sinus is the principal vein of the superficial venous tree of the human brain [23], draining the blood of the veins located at the surface of the cortex. Its correct segmentation is then necessary for the detection of this whole vascular tree, more especially if correct topological properties have to be recovered. The superior sagittal sinus presents many invariant properties (*i.e.* properties being identical for every subject) which can be useful for guiding a segmentation

process. Some of these properties and possible ways to use them are described in the following subsections.

3.1 Trajectory properties: A way to guide normal planes computation

The superior sagittal sinus presents a regular trajectory illustrated in Fig. 1. It is located in the sagittal median plane of the brain (this plane being defined by the frontier between both cerebral hemispheres) and is quite parallel to the surface of the head. This trajectory theoretically enables to compute successive cross-section planes being perpendicular to the sinus axis. Indeed, if the surface of the head and the sagittal median plane of the brain can be found, then their intersection provides a curve. A normal plane computation using the points of this curve finally gives planes being also normal to the sinus axis. This strategy can then be used to perform a slice by slice segmentation of the sinus.
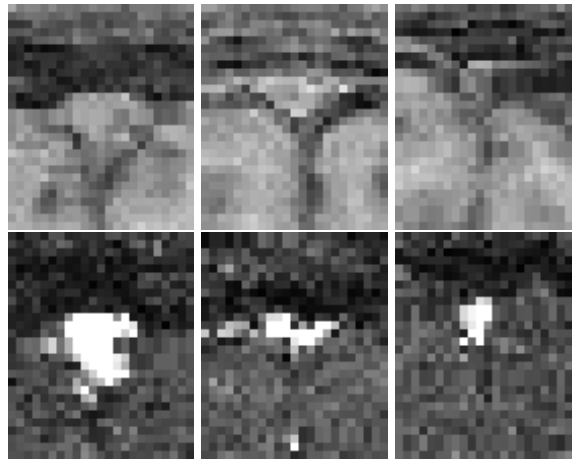

Fig. 2. Slices of MRA and MRI data at various positions on the superior sagittal sinus. Top: MRI slices. Bottom: MRA slices. The slices of the same column correspond to the same position. Flowing blood: in white in MRA slices, and in light grey (with the *dura mater*) in MRI ones. Brain hemispheres: in light grey in the inferior part of MRI slices. Skull: in light grey in the superior part of MRI slices.

3.2 Structure intensity and relative positions: A way to guide watershed segmentation

Observing MRA slices such as the ones illustrated in the second row of Fig. 2, it can be seen that the flowing blood is quite visible, being the only structure presenting the highest intensity. In MRI slices, illustrated in the first row of Fig. 2, more structures can be observed in an easier way. Although the flowing blood does not present a very high intensity in such slices, it can be observed surrounded by the *dura mater*. The brain hemispheres present a nearly identical intensity, such as part

of the skull. These four structures are separated by areas of low intensity and their relative positions are globally invariant.

MRA and MRI intensity properties can then be used to perform watershed segmentation on slices of the superior sagittal sinus region. Indeed, a gradient computation on MRA data should correctly delineate the blood from the remaining structures. A watershed segmentation could also be directly used on MRI data to segment the different structures (considering low intensity regions as the frontier between them). Since the main problem of watershed segmentation remains oversegmentation, it is important to choose correct markers to initialise it. This could be done here by sharing information between MRA and MRI segmentation (the segmentation of blood in MRA could be used to find a marker for the *dura mater* in MRI, and vice versa) or by sharing information between successive MRI or MRA segmentations.

3.3 Structure homogeneity along the sinus trajectory: Justifying an iterative slice by slice strategy

The sinus and its neighbouring structures present quite invariant position properties. By considering slices at different points on the superior sagittal sinus trajectory, it can also be observed that their size and distance from each other are different but vary quite smoothly, as illustrated in the three views of Fig. 2. This property could be efficiently used to start from one slice and successively generate markers to initialise segmentation of the neighbouring ones. Such a strategy is generally proposed in vessel tracking algorithms [24]. The main weakness of vessel tracking approaches is that a segmentation error in one slice will generally propagate in all the following ones. In order to avoid such problems, an alternative solution could be to propose an iterative approach. For each slice, it consists in first segmenting an average image of the current slice and its neighbours. The obtained result can then be used to generate markers for a new segmentation of a new average slice, closer to the current one. This process can then be iterated until segmenting the real slice.

4 Method

The method proposed in this section uses the different pieces of knowledge previously described in order to take advantage of them and to propose a multimodal segmentation process.

4.1 Input and output

This method takes as input a T_1 MRI and a TOF MRA of the same patient [1] . They must contain at least the top of head and have to be correctly superimposed. If they are not, superimposition can be obtained by performing a rigid registration (using translations and rotations). An example of data used by the method is illustrated in Fig. 1. The method provides two resulting (binary) images: an image of the flowing blood segmented in the MRA data and a segmentation of the *dura mater* surrounding the blood and then forming the sinus wall, segmented from the MRI data.
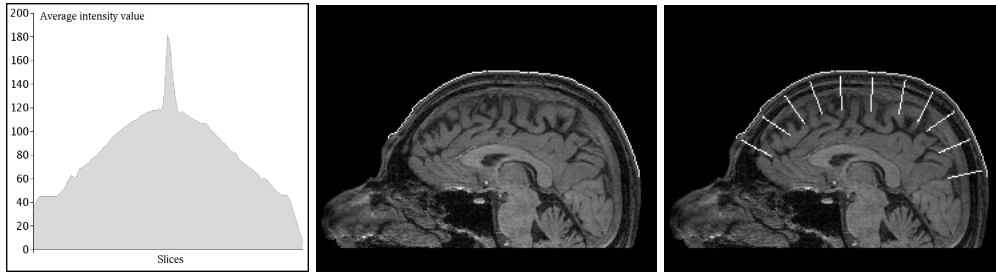

Fig. 3. Computation of the slices $\{s_i^{mra}\}_{i=0}^t$ and $\{s_i^{mri}\}_{i=0}^t$. Left: histogram of average intensity values of TOF MRA sagittal slices. The peak clearly identifies the vascular signal of the superior sagittal sinus, then enabling to localise the slice corresponding to the superior sagittal sinus axis. Middle: curve obtained by intersecting the head surface and the sagittal slice previously detected (in white). Right: subset of slices obtained by computing the discrete planes being normal to this curve (in white).

4.2 Preprocessing

The segmentation process is not carried out on the whole images, but on slices that must be normal to the sinus axis. A first step then consists in computing these slices. The sinus axis is parallel to a curve obtained by intersecting the cerebral sagittal median plane and the head surface. The surface of the head can be easily found by many interactive or automatic methods. The automatic one proposed here is based on an Otsu thresholding process preserving the largest binary connected component. The sagittal median plane of the brain can be found by an histogram analysis of the MRA sagittal slice average intensities (left part of Fig. 3). In order to deal with data where the medial slices are not perfectly fitting the cerebral medial planes, slices obtained by rotation along the vertical axis with a discrete set of angles included in $[-\pi/12, \pi/12]$ are also considered. The intersection of the plane of highest intensity and the surface of the head then provides a discrete curve. Normal vector computation on points regularly sampled on this curve finally enables

---

[1] This couple of data could be replaced by PC MRA magnitude and phase images, which present quite similar intensity properties.

to compute planes being normal to the curve and then to the sinus axis.

This step provides two sets of slices of the superior sagittal sinus, defined by the normal planes previously computed. The first set is composed of MRI slices while the second contains MRA ones, the n-th slice of the first set corresponding to the n-th slice of the second. It has been experimentally observed that sets of 256 slices were sufficient to carry out the segmentation of millimetric data. Moreover, they are sampled to only keep 23×28 voxel-slices located 10 mm away [2] from the head surface, assuming that small slices centred on the sinus and containing neighbouring structures enable to obtain correct results with a lower computation time.

4.3 Algorithm

4.3.1 Definitions and notations

In the following, a 2D slice of $n \times m$ voxels is considered as a function $[0, n-1] \times [0, m-1] \to \mathbb{N}$. Let $\{s_i^{mra}\}_{i=0}^t$ and $\{s_i^{mri}\}_{i=0}^t$ be sequences of MRA and MRI slices such that for all $a, b, c \in [0, t]$ with $a < b < c$ the slice s_b^α is physically located between s_a^α and s_c^α (with $\alpha \in \{mra, mri\}$). For each $i \in [0, t]$, let $\{I_k^i\}_{k=0}^\omega$ be a sequence of intervals around i, decreasing from $[0, t]$ to $\{i\}$ and verifying:

$$I_0^i = [0, t],$$

$$\forall x, y \in [0, \omega], x < y \Rightarrow I_y^i \subset I_x^i,$$

$$I_\omega^i = [i, i].$$

For each $i \in [0, t]$ let $\{s_{i,k}^{mra}\}_{k=0}^\omega$ and $\{s_{i,k}^{mri}\}_{k=0}^\omega$ be the averaged sequences over I_k^i:

$$s_{i,k}^\alpha = \frac{1}{|I_k^i|} \sum_{m \in I_k^i} s_m^\alpha,$$

with $|I|$ standing for the length of an interval I. For $i \in [0, t]$, the result of the segmentation of s_i^α is denoted by b_i^α, which can be defined as a label image:

$$b_i^\alpha : [0, n-1] \times [0, m-1] \to \{v, m, s, f\},$$

---

[2] The 10 mm value has been experimentally determined for brains of normal size. For brains presenting a much different size, such as those of children, this value should be adapted. As an example, a solution could consist in multiplying this length by a factor $\sqrt[3]{V/1200}$ where V cm^3 represents the volume of the studied brain (the averaged volume for an adult brain being 1200 cm^3). In the same way, the 23×28 voxel size of the considered slices is designed to fit data composed of millimetric voxels and should then be adapted according to the image resolution.

where v, m, s, f correspond to the vascular structures (flowing blood, *dura mater*), the non-vascular ones (skull, brain), the area separating these structures (cerebrospinal fluid) and the watershed frontiers, respectively. Similarly, for $i \in [0, t]$ and $k \in [0, \omega]$, the result of the segmentation of $s_{i,k}^{\alpha}$ is denoted $b_{i,k}^{\alpha}$. It then has to be noticed that:

$$b_{i,\omega}^{\alpha} = b_i^{\alpha},$$

and that the searched binary structures are provided by $(b_i^{mra})^{-1}(\{v\})$ (flowing blood) and $(b_i^{mri})^{-1}(\{v\})$ (blood and *dura mater*).

4.3.2   *General description*

For each slice s_i^{mra} two sequences $\{s_{i,k}^{mra}\}_{k=0}^{\omega}$ and $\{s_{i,k}^{mri}\}_{i=0}^{\omega}$ are then defined. These sequences start from an average image of all the MRA and MRI slices, and finally come to the *i*-th MRA and MRI slice, respectively. Assuming that both sequences will smoothly converge from an average image to the current slice, the following segmentation strategy based on an iterative process is proposed:

(1) initial segmentation of $s_{i,0}^{mra}$ and $s_{i,0}^{mri}$, providing $b_{i,0}^{mra}$ and $b_{i,0}^{mri}$;
(2) for $k = 1$ to ω:
    (a) segmentation of $s_{i,k}^{mri}$, using $b_{i,k-1}^{mra}$ and $b_{i,k-1}^{mri}$, providing $b_{i,k}^{mri}$;
    (b) segmentation of $s_{i,k}^{mra}$, using $b_{i,k}^{mri}$, providing $b_{i,k}^{mra}$.

The process starts from average images and iteratively uses previous segmentations of both modalities to carry out the current segmentation. This one is performed by using a watershed algorithm while previous segmentations are used for creation of markers dedicated to watershed initialisation. In the following paragraphs, the segmentation process is more precisely described. The gradient computation and markers creation steps are explained in specific paragraphs.

4.3.3   *Initialisation*

This first step of the method consists in performing the segmentation of $s_{i,0}^{mra}$ and $s_{i,0}^{mri}$ for $i \in [0, \omega]$. By definition, for all $i, j \in [0, \omega]$, $s_{i,0}^{\alpha} = s_{j,0}^{\alpha}$. Thus the initialisation step only requires to segment two average slices, one for the MRA and the MRI data. The initialisation, illustrated in Fig. 4, is organised as follows:

(1) grey-level opening of the MRA slice with a flat structuring element (3×3 cross): the points of maximum value become the markers for the flowing blood in the MRA and MRI slices;
(2) successive grey-level openings of the MRI slice with three flat structuring elements (a one-voxel wide line and two 7×7 circular elements): the points

9

of maximum value become the markers for the brain and the bone in the MRI slices;

(3) watershed segmentation of the MRI slice using the four markers, providing a first image $(b_{i,0}^{mri})'$;

(4) gradient computation of the MRI slice and watershed segmentation of the gradient MRI slice using the four markers plus a new marker $((b_{i,0}^{mri})')^{-1}(\{f\})$ provided by the frontier between the four regions of the previous segmentation, generating $b_{i,0}^{mri}$;

(5) gradient computation of the MRA slice and watershed segmentation of the gradient MRA slice using one marker plus a new marker provided by the frontier between the four regions of the first MRI segmentation, generating $b_{i,0}^{mra}$.

Standard shape and size of the different structuring elements have been chosen in order to fit the different structures to find. That step finally provides $b_{i,0}^{mri}$ and $b_{i,0}^{mra}$ then enabling to initialise the iterative process for each $i \in [0, t]$.

(a)   (b)   (c)   (d)   (e)
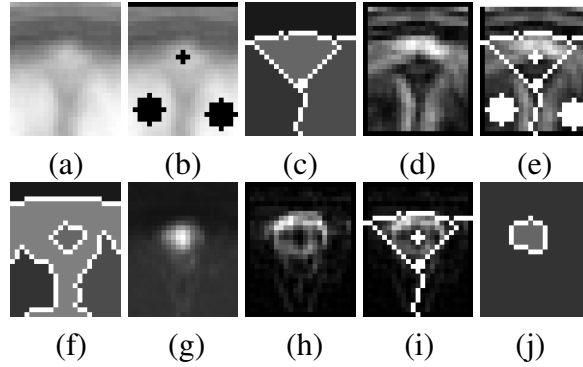
(f)   (g)   (h)   (i)   (j)

Fig. 4. Initialisation process. (a) MRI average slice ($s_{i,0}^{mri}$). (b) MRI with four markers. (c) First segmentation $(b_{i,0}^{mri})'$. (d) MRI gradient. (e) MRI gradient with five markers. (f) Final MRI segmentation ($b_{i,0}^{mri}$). (g) MRA average slice ($s_{i,0}^{mra}$). (h) MRA gradient. (i) MRA gradient with two markers. (j) MRA segmentation ($b_{i,0}^{mra}$).

4.3.4 Iterative process

For each $i \in [0, t]$, at the step k, the iterative process consists in first segmenting the current MRI slice ($s_{i,k}^{mri}$) by using the MRA and MRI segmentation of the previous step ($b_{i,k-1}^{mra}$ and $b_{i,k-1}^{mri}$). Then the current MRA slice can be segmented using the current MRI segmentation ($b_{i,k}^{mri}$). A step calculating $b_{i,k}^{mra}$ and $b_{i,k}^{mri}$, illustrated in Fig. 5 can be decomposed as follows (the marker generation for this iterative step is described in Subsection 4.3.6):

(1) creation of two markers to initialise $s_{i,k}^{mri}$ segmentation;

(2) watershed segmentation of $s_{i,k}^{mri}$, using the two markers, generating a first image $(b_{i,k}^{mri})'$;

10

(3) gradient computation of $s_{i,k}^{mri}$ and watershed segmentation of $s_{i,k}^{mri}$ gradient, using the two markers plus one marker $((b_{i,k}^{mri})')^{-1}(\{f\})$ provided by the frontier of the previous watershed segmentation, generating $b_{i,k}^{mri}$;

(4) creation of two markers to initialise $s_{i,k}^{mra}$ segmentation;

(5) gradient computation of $s_{i,k}^{mra}$ and watershed segmentation of $s_{i,k}^{mra}$ gradient, using the two markers, generating $b_{i,k}^{mra}$.

(a)   (b)   (c)   (d)   (e)
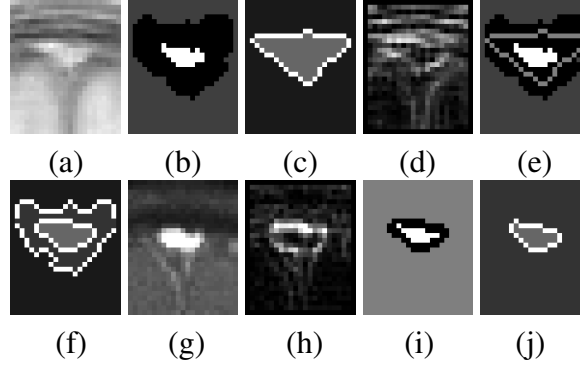
(f)   (g)   (h)   (i)   (j)

Fig. 5. A step of the iterative process for one slice. (a) MRI average slice ($s_{i,k}^{mri}$). (b) Two markers for MRI segmentation. (c) First segmentation ($b_{i,k}^{mri}$)'. (d) MRI gradient. (e) Two markers plus the one obtained from the first segmentation. (f) Final MRI segmentation ($b_{i,k}^{mri}$). (g) MRA average slice ($s_{i,k}^{mra}$). (h) MRA gradient. (i) Two markers for MRA segmentation. (j) MRA segmentation ($b_{i,k}^{mra}$).

4.3.5   Gradient computation

For each step, the segmentation of both MRA and MRI slices requires the computation of gradient images. Concerning the MRI slices, the gradient is computed by choosing the maximum intensity variation in the four principal directions, then correctly delineating the main structures from the low intensity regions. This gradient calculation, illustrated in pictures (d) of Figs. 4 and 5 gives correct results as the different regions of interest have homogeneous intensity levels. This is not the case for the flowing blood in the MRA slices, which presents a very high but quite heterogeneous level. Since computing a simple gradient does not provide well defined frontiers, a solution consists in dividing the gradient value calculated at a pixel by the pixel value. This normalised gradient, illustrated in pictures (h) of Figs. 4 and 5, will present low values in homogeneous high intensity regions and high values for the background points located at the frontier with the flowing blood.

4.3.6   Marker generation

At each step $k \in [1, \omega]$ of the iterative process and for each slice s_i^α ($i \in [0, t]$), it is necessary to generate markers to initialise the different watershed segmentations of $s_{i,k}^{mri}$ and $s_{i,k}^{mra}$. In the previous version of the method [5], markers were generated by only taking into account information related to the current slice s_i^α and its previous

segmentations $b_{i,k-1}^{mri}$ and $b_{i,k-1}^{mra}$. In this new version, the markers for all slices s_i^α ($i \in [0, t]$) are generated during the same process. This new marker generation strategy, which is designed to integrate continuity and regularity constraints in the segmentation process, assumes that the slice sequences $\{b_{i,k-1}^{mri}\}_{i=0}^t$ and $\{b_{i,k-1}^{mra}\}_{i=0}^t$ can be considered as 3D images of the segmented structures at step $k-1$ by stacking them. Such 3D images are then defined by:

$$\left|\begin{array}{rcl} B_{k-1}^\alpha : [0,t] \times [0, n-1] \times [0, m-1] & \to & \mathbb{N} \\ (i, x, y) & \mapsto & b_{i,k-1}^\alpha(x, y) \end{array}\right. .$$

The generation of the different markers for watershed segmentation at step k is then performed as follows.

The segmentation of the MRI slice requires two markers: one for vascular structures (the blood and the surrounding *dura mater*), and one for non-vascular ones (brain hemispheres and skull). The first (vascular) marker is chosen as being the vascular part segmented in B_{k-1}^{mra} *i.e.* $(B_{k-1}^{mra})^{-1}(\{v\})$. The second marker is obtained by first considering the 3D object corresponding to the non-vascular part of B_{k-1}^{mri} *i.e.* $(B_{k-1}^{mri})^{-1}(\{m\})$ (for marker generation from B_0^{mri}, the different parts corresponding to the skull and both hemispheres are assumed to correspond to the label m). All simple points [25] of $(B_{k-1}^{mri})^{-1}(\{m\})$ are then removed [3], except points located at the border of the image. Examples of both markers are illustrated in picture (b) of Fig. 5.

The segmentation of the MRA slice also requires two markers: one for vascular structures (the flowing blood), and one for non-vascular ones (all other structures) The first (vascular) marker is obtained by first considering the 3D object corresponding to the vascular part of B_k^{mri}, *i.e.* $(B_k^{mri})^{-1}(\{v\})$. All simple points of $(B_k^{mri})^{-1}(\{v\})$ are then removed. All 3D simple points located at the border of this object are then removed, except points also located at the border of the image. The second (non-vascular) marker is chosen as being the complement of the vascular part segmented in B_k^{mri}, *i.e.* $(B_k^{mri})^{-1}(\overline{\{v\}})$. Examples of both markers are illustrated in picture (i) of Fig. 5.

It has to be noticed that, by definition, the 3D binary object corresponding to the vascular part of B_0^{mra}, *i.e.* $(B_0^{mra})^{-1}(\{v\})$, is necessarily composed of one connected component with no hole and no cavity. The use of topology preserving reduction during the vascular marker generation process and the successive 2D slice by slice segmentation then guarantees that the obtained vascular objects of $(B_\omega^{mra})^{-1}(\{v\})$ and $(B_\omega^{mri})^{-1}(\{v\})$ will also present the same properties, thus providing a satisfy-

---

[3] These points have to be 3D simple with respect to B, but also 2D simple with respect to b in order to preserve correct properties in the 2D slices. This remark is also valid for the reduction of the next paragraph.

ing topology to the final result. The removal of border points during the vascular marker generation only also guarantees that the segmentation will be performed in a smooth way. Finally, the proposed iterative process also imposes that the flowing blood segmented from MRA data is necessarily included in the sinus segmented from MRI data:

$$(b_i^{mra})^{-1}(\{v\}) \subseteq (b_i^{mri})^{-1}(\{v\}),$$

thus preserving correct anatomical properties.

4.4 Postprocessing

The segmentation then provides two sets of slices corresponding to the segmentation of the flowing blood in the MRA data set and to the segmentation of the sinus blood and wall in the MRI data set, respectively. These slices have then to be put back to their correct position in the initial images. During this step, it might happen that small gaps appear between successive slices. Since these gaps are quite small (their thickness is never larger than one voxel), they can then be filled by using a binary closing with a linear structuring element composed of 3 voxels and oriented according to the direction of the superior sagittal sinus axis. As a very last step, the user can also choose to apply a binary opening to smooth the image (for example by using a $3 \times 3 \times 3$ cross). It has to be noticed that other solutions to finally generate the superior sagittal sinus wall and flowing blood could be considered. As an example, a postprocessing no longer based on mathematical morphology but on geometrical models could consist in generating a tubular model parameterised by the set of cross sections provided by the sets of slices.

5 Experimental section

5.1 Data acquisition

A database of 9 couples of images (T_1 MRI/TOF MRA) has been used to validate the efficiency of the proposed algorithm. Both TOF MRA and T_1 MRI exams were performed on a 2 Tesla whole-body imager (Tomikon S200 Bruker) using a head transmitter and receiver RF coil. T_1 MRI data are composed of $180 \times 256 \times 256$ cubical voxels of 1 mm edges. TOF MRA data are composed of $256 \times 70 \times 256$ anisotropic voxels of dimensions $0.75 \times 1 \times 1$ mm. Since both acquisitions were performed during the same exams for each couple of data, it has been possible to perform a rigid registration and to undersample MRA data by only using the phys-

ical parameters of the imaging process, in order to obtain isotropic and registered data.

5.2 *Complexity and computation time*

The algorithm presented in this paper has been implemented on the Medimax medical image processing platform[4] and is mainly based on the ImLib3D [26] open source C++ library[5]. The preprocessing step (excluding registration), the algorithm and the postprocessing step present algorithmic complexities equal to $O(\max\{X, \theta\}.Y.Z)$, $O(\omega.t.n.m)$ and $O(t.x.y)$, respectively, where θ is the number of rotation angles used for determining the cerebral medial plane, ω is the number of iterations, t is the number of slices, n, m are the slice dimensions and X, Y, Z are the MR data dimensions. In the proposed experiments values $\theta = 20$, $\omega = 50$, $n = 23$, $m = 28$, and $t = 256$ have been chosen in order to fit the millimetric resolution of the images. The images have been segmented with a computer using a 2.4 GHz Pentium IV processor with 2 GB of memory. The average computation time is then 5 minutes. It has to be noticed that the proposed algorithm runs in an entirely automatic fashion.
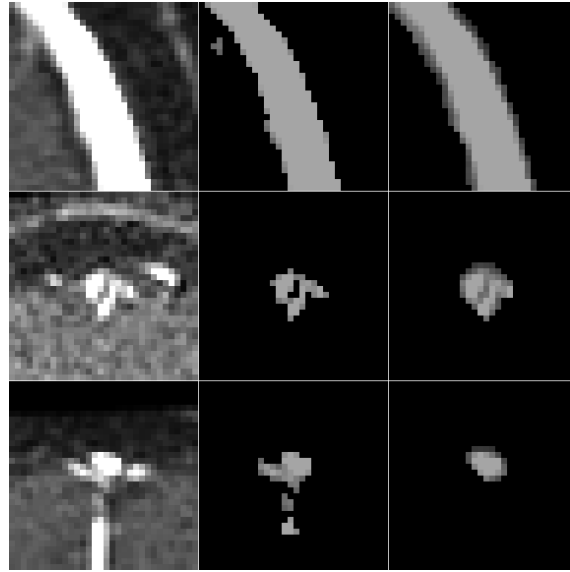

Fig. 6. Results provided by the proposed method and a region-growing method. First column: MRA data. Second column: region-growing segmentation. Third column: proposed segmentation. First row: sagittal view. Second end third rows: coronal views.

14

6 Results and discussion

The results obtained with the proposed method, illustrated in Figs. 6 and 7, have been compared to those provided by a region-growing algorithm proposed in [4]. All the validations have been carried out by a human specialist who qualitatively tested both algorithms on each case of the previously described database.

During the validation, it has been observed that the proposed method could segment the flowing blood even when MRA signal was heterogeneous or low. For most of vessel segmentation methods (often relying on strategies essentially based on intensity criteria) perturbation of MRA signal generally provokes segmentation errors. Such perturbations, which can be caused by aliasing artifacts (inherent to the chosen blood flow velocity interval visualised in MRA) or by turbulences disturbing the laminar properties of the flow and thus its correct visualisation, usually forbid a correct segmentation of the whole flowing blood signal. However, since the proposed method uses not only angiographic (MRA) but also non-angiographic (MRI) data, it can use this supplementary information to guide the segmentation process even when the flowing blood signal becomes too low to be sufficient for segmentation. This strategy finally enables to obtain results which are much less dependent of the homogeneity and quality of the flowing blood signal, as illustrated in the second row of Fig. 6.

For highly homogeneous intensity regions, it has been observed that both algorithms provide correct segmentations. However, as illustrated in the first row of Fig. 6, the proposed method tends to oversegment (*i.e.* to segment border voxels presenting partial volume effects) the blood flow, while the region growing one tends to undersegment it. Determining which method presents the best results for border voxels is not an easy task [27]. Nevertheless, the behaviour of the proposed method can be considered as satisfactory since the obtained segmentation enables to use the binary image as a reliable mask for removal of noisy and non vascular part of the MRA data.

Moreover, the proposed algorithm is able to specifically segment the sinus while the region-growing algorithm also segments connected veins, as observed in the third row of Fig. 6. This ability to discriminate a specific vascular structure is an interesting property. Indeed, segmentation methods able to segment a precise vessel or set of vessels avoid the further use of labelling processes in order to localise given structures. This can be useful for applications requiring such knowledge, as neurosurgery planning or functional analysis. In the case of this method, the segmentation of the sinus could also be used to correctly initialise more general segmentation processes devoted to the whole superficial venous tree such as the one proposed in [28].

It has to be noticed that the optimised version described in this paper presents two

15

main improvements by comparison to the initial version detailed in [5]. Indeed, the use of an homotopic reduction for marker generation at each step of the iterative process avoids infrequent but possibly erroneous segmentation phenomena (non-continuity, lack of regularity) which could happen on isolated slices, by constraining each segmented slice to present homogeneous properties with respect to its neighbours. This optimisation finally induces a more satisfying behaviour of the method in terms of continuity and of regularity, (*i.e.* in terms of anatomical coherence) of the segmented structures.

Finally, these validations prove that the method described in this paper enables to obtain satisfactory results for the segmentation of the superior sagittal sinus. This can be explained by the use of supplementary information, provided by high level *a-priori* knowledge related to anatomical properties, but also by multimodal (angiographic and non-angiographic) data. The use of such kind of knowledge, illustrated in this paper on a precise vessel, could be extended to other vascular structures and involved in different image processing strategies, leading to a new vessel segmentation methodology being closer to the way radiologists analyse angiographic data. However, it has to be pointed out that the use of *a-priori* knowledge and of non-angiographic data for vessel segmentation is probably much more adapted to segmentation of structures without pathologies (for application in neurosurgery planning or landmark detection) than to vascular pathology diagnosis, which strongly relies on the analysis of flowing blood signal, the perturbation of which can enable to characterise aneurysms or stenoses.

7 Conclusion

This paper presents an optimised version of a novel method, based on watershed segmentation and mathematical morphology operators guided by anatomical knowledge. This method is dedicated to superior sagittal sinus segmentation from brain multimodal MR data. It has been tested on 9 cases, providing more precise results than a previously proposed region-growing algorithm, even in case of strong inhomogeneity of signal in MRA data. The main originality of this work consists in integrating high level anatomical knowledge, and using both MRA and MRI data in order to guide mathematical morphology tools. A first attempt to integrate anatomical knowledge in a vessel segmentation process had already been proposed in [4], where an atlas was used to divide the brain into areas having homogeneous vascular properties. The method proposed here can be considered as being dedicated to one of these areas (the superior sagittal sinus area), then proposing a reliable strategy for the vessels it contains. This work is part of a new kind of segmentation strategy consisting in processing each part of a vascular tree in a adapted fashion, instead of processing all the vessels in a global way. Further work will now consist in using this method as a first step for segmentation and topology recovery of the whole cerebral superficial venous tree.
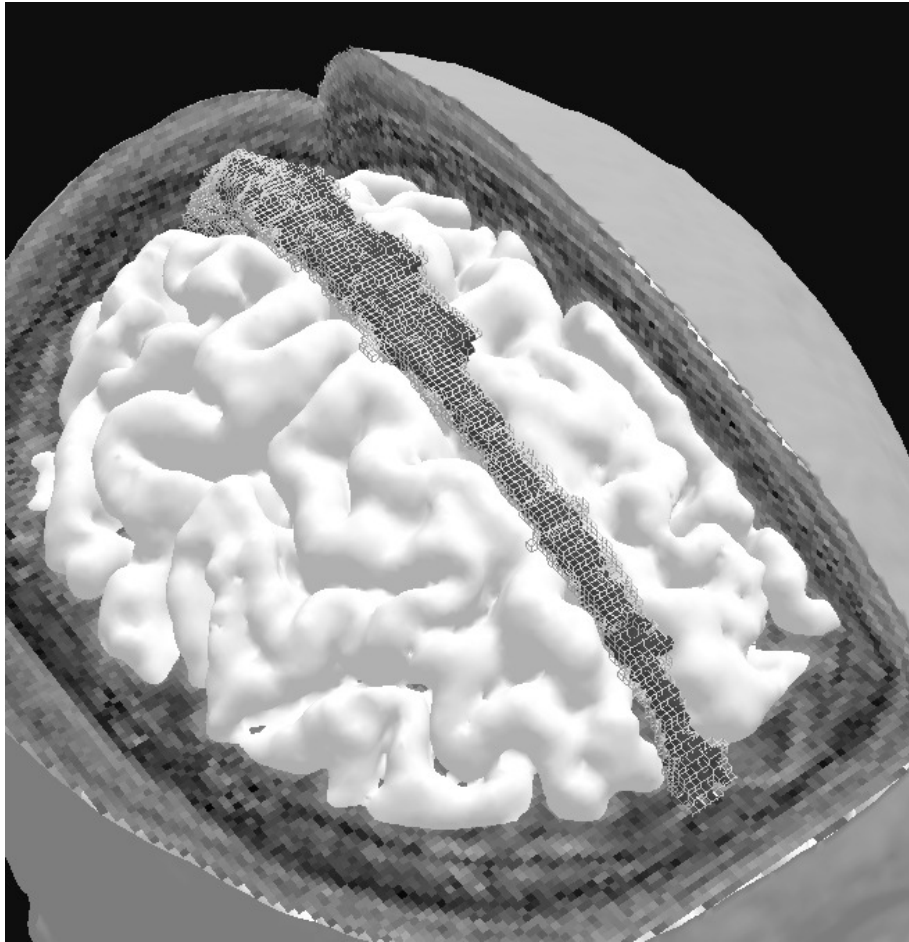
Fig. 7. Flowing blood (in dark grey) surrounded by the superior sagittal sinus wall (light grey mesh).

Acknowledgements

References

[1] C. Dumoulin, H. Hart, Magnetic resonance angiography, Radiology 161 (3) (1986) 717–720.

[2] F. Wehrli, A. Shimakawa, G. Gullberg, J. McFall, Time of flight MR flow imaging:

Selective saturation recovery with gradient refocusing, Radiology 160 (3) (1986) 781–785.

[3] C. Dumoulin, S. Souza, M. Walker, W. Wagle, Three-dimensional phase contrast angiography, Magnetic Resonance in Medicine 9 (1) (1989) 139–149.

[4] N. Passat, C. Ronse, J. Baruthio, J.-P. Armspach, C. Maillot, C. Jahn, Region-growing segmentation of brain vessels: An atlas-based automatic approach, Journal of Magnetic Resonance Imaging 21 (6) (2005) 715–725.

[5] N. Passat, C. Ronse, J. Baruthio, J.-P. Armspach, J. Foucher, Using watershed and multimodal data for vessel segmentation: Application to the superior sagittal sinus, in: C. Ronse, L. Najman, É. Decencière (Eds.), Mathematical Morphology: 40 years on. Proceedings of the 7th International Symposium on Mathematical Morphology, Vol. 30 of Computational Imaging and Vision, Springer SBM, Paris, France, 2005, pp. 419–428.

[6] C. Kirbas, F. Quek, A review of vessel extraction techniques and algorithms, ACM Computing Surveys 36 (2) (2004) 81–121.

[7] J. Suri, K. Liu, L. Reden, S. Laxminarayan, A review on MR vascular image processing: Skeleton versus nonskeleton approaches: Part II, IEEE Transactions on Information Technology in Biomedicine 6 (4) (2002) 338–350.

[8] G. Gerig, T. Koller, G. Székely, C. Brechbühler, O. Kübler, Symbolic description of 3-D structures applied to cerebral vessel tree obtained from MR angiography volume data, in: H. Barrett, A. Gmitro (Eds.), Information Processing in Medical Imaging - IPMI 1993, 13th International Conference, Proceedings, Vol. 687 of Lecture Notes in Computer Science, Springer, Flagstaff, Arizona, USA, 1993, pp. 94–111.

[9] M. Wilkinson, T. Wijbenga, G. de Vries, M. Westenberg, Blood vessel segmentation using moving-window robust automatic threshold selection, in: International Conference on Image Processing - ICIP 2003, 10th International Conference, Proceedings, Vol. 2, IEEE Signal Processing Society, Barcelona, Spain, 2003, pp. 1093–1096.

[10] H. Cline, D. Thedens, P. Irarrazaval, C. Meyer, B. Hu, D. Nishimura, S. Ludke, 3D MR coronary artery segmentation, Magnetic Resonance in Medicine 40 (5) (1998) 697–702.

[11] H. Cline, D. Thedens, C. Meyer, D. Nishimura, T. Foo, S. Ludke, Combined connectivity and a gray-level morphological filter in magnetic resonance coronary angiography, Magnetic Resonance in Medicine 43 (6) (2000) 892–895.

[12] P. Yim, P. Choyke, R. Summers, Gray-scale skeletonization of small vessels in magnetic resonance angiography, IEEE Transactions on Medical Imaging 19 (6) (2000) 568–576.

[13] C. Zahlten, H. Jürgens, C. Evertsz, R. Leppek, H.-O. Peitgen, K. Klose, Portal vein reconstruction based on topology, European Journal of Radiology 19 (2) (1995) 96–100.

18

[14] P. Dokládal, C. Lohou, L. Perroton, G. Bertrand, Liver blood vessels extraction by a 3-D topological approach, in: C. Taylor, A. Colchester (Eds.), Medical Image Computing and Computer-Assisted Intervention - MICCAI 1999, 2nd International Conference, Proceedings, Vol. 1679 of Lecture Notes in Computer Science, Springer, Cambridge, United Kingdom, 1999, pp. 98–105.

[15] S. Kobashi, Y. Hata, Y. Tokimoto, M. Ishikawa, Automatic segmentation of blood vessels from MR angiography volume data by using fuzzy logic technique, in: K. Hanson (Ed.), Medical Imaging: Image Processing 1999, Proceedings, Vol. 3661, SPIE, San Diego, California, USA, 1999, pp. 968–976.

[16] S. Kobashi, N. Kamiura, Y. Hata, F. Miyawaki, Volume-quantization-based neural network approach to 3D MR angiography image segmentation, Image and Vision Computing 19 (4) (2001) 185–193.

[17] N. Passat, C. Ronse, J. Baruthio, J.-P. Armspach, Automatic parameterization of grey-level hit-or-miss operators for brain vessel segmentation, in: International Conference on Acoustics, Speech, and Signal Processing - ICASSP 2005, 30th International Conference, Proceedings, Vol. 2, IEEE Signal Processing Society, Philadelphia, Pennsylvania, USA, 2005, pp. 737–740.

[18] N. Passat, C. Ronse, J. Baruthio, J.-P. Armspach, C. Maillot, Magnetic resonance angiography: From anatomical knowledge modeling to vessel segmentation, Medical Image Analysis, in Press.

[19] B. Naegel, C. Ronse, L. Soler, Using grey-scale hit-or-miss transform for segmenting the portal network of the liver, in: C. Ronse, L. Najman, É. Decencière (Eds.), Mathematical Morphology: 40 years on. Proceedings of the 7th International Symposium on Mathematical Morphology, Vol. 30 of Computational Imaging and Vision, Springer SBM, Paris, France, 2005, pp. 429–440.

[20] A. Sanderson, D. Parker, T. Henderson, Simultaneous segmentation of MR and X-ray angiograms for visualization of cerebral vascular anatomy, in: M. Viergever (Ed.), International Conference on Volume Image Processing - VIP 1993, 4th International Conference, Proceedings, SCVR, Utrecht, Netherlands, 1993, pp. 11–14.

[21] C. Pellot, I. Bloch, A. Herment, F. Sureda, An attempt to 3D reconstruct vessel morphology from X-ray projections and intravascular ultrasounds modeling and fusion, Computerized Medical Imaging and Graphics 20 (3) (1996) 141–151.

[22] S. Beucher, F. Meyer, The morphological approach to segmentation: The watershed transformation, in: E. Dougherty (Ed.), Mathematical Morphology in Image Processing, Marcel Dekker, New York, 1992, pp. 433–481.

[23] J. Nolte, The Human Brain - An Introduction to its Functional Anatomy, Elsevier Science, 2001, Ch. 6, pp. 119–145.

[24] O. Wink, W. Niessen, M. Viergever, Fast delineation and visualization of vessels in 3D angiographic images, IEEE Transactions on Medical Imaging 19 (4) (2000) 337–346.

[25] G. Bertrand, A Boolean characterization of three-dimensional simple points, Pattern Recognition Letters 17 (2) (1996) 115–124.

[26] M. Bosc, T. Vik, J.-P. Armspach, F. Heitz, ImLib3D: An efficient, open source, medical image processing framework in C++, in: R. Ellis, T. Peters (Eds.), Medical Image Computing and Computer-Assisted Intervention - MICCAI 2003, 6th International Conference, Proceedings, Part II, Vol. 2879 of Lecture Notes in Computer Science, Springer, Montréal, Canada, 2003, pp. 981–982.

[27] R. Hoogeveen, C. Bakker, M. Viergever, Limits to the accuracy of vessel diameter measurement in MR angiography, Journal of Magnetic Resonance Imaging 8 (6) (1998) 1228–1235.

[28] N. Passat, C. Ronse, J. Baruthio, J.-P. Armspach, M. Bosc, J. Foucher, Using multimodal MR data for segmentation and topology recovery of the cerebral superficial venous tree, in: G. Bebis, R. Boyle, D. Koracin, B. Parvin (Eds.), International Symposium on Visual Computing - ISVC'05, 1st International Symposium, Proceedings, Vol. 3804 of Lecture Notes in Computer Science, Springer, Lake Tahoe, Nevada, USA, 2005, pp. 60–67.